J. Fluid Mech. (2010), *vol.* 645, *pp.* 295–314.
doi:10.1017/S0022112009992643

Local balance and cross-scale flux of available potential energy

M. JEROEN MOLEMAKER† AND JAMES C. MCWILLIAMS

Institute of Geophysics and Planetary Physics, UCLA Los Angeles, CA 90095-1567, USA

(Received 7 February 2008; revised 30 September 2009; accepted 4 October 2009; first published online 8 February 2010)

Gravitational available potential energy is a central concept in an energy analysis of flows in which buoyancy effects are dynamically important. These include, but are not limited to, most geophysical flows with persistently stable density stratification. The volume-integrated available potential energy $\mathscr{E}_{ap}$ is defined as the difference between the gravitational potential energy of the system and the potential energy of a reference state with the lowest potential energy that can be reached by adiabatic material rearrangement; $\mathscr{E}_{ap}$ determines how much energy is available for conservative dynamical exchange with kinetic energy $\mathscr{E}_k$. In this paper we introduce new techniques for computing the local available potential energy density E_{ap} in numerical simulations that allow for a more accurate and complete analysis of the available potential energy and its dynamical balances as part of the complete energy cycle of a flow. In particular, the definition of E_{ap} and an associated gravitation disturbance field $\mathscr{A}$ permit us to make a spectral decomposition of its dynamical balance and examine the cross-scale energy flux. Several examples illustrate the spatial structure of E_{ap} and its evolutionary influences. The greatest attention is given to an analysis of a turbulent-equilibrium simulation Eady-like vertical-shear flow with rotation and stable stratification. In this regime E_{ap} exhibits a vigorous forward energy cascade from the mesoscale through the submesoscale range – first in a scale range dominated by frontogenesis and positive buoyancy-flux conversion from $\mathscr{E}_{ap}$ to $\mathscr{E}_k$ and then, after strong frontal instability and frontogenetic arrest, in a coupled kinetic-potential energy inertial-cascade range with negative buoyancy-flux conversion – *en route* to fine-scale dissipation of both energy components.

1. Introduction

Lorenz (1955) formalized the concept of available potential energy (APE), which has proved to be very useful in analyses of energy in the atmospheric and oceanic general circulations as the appropriate companion to kinetic energy (KE) for weakly non-conservative dynamical processes (Lorenz 1967; Huang 1998). APE has also been shown to be a useful quantity for smaller-scale stratified flows (Winters *et al.* 1995). The concept is applicable to geometrically complex, simply connected domains (i.e. including topographic variations), and it is useful even in strongly diabatic and unstably stratified regimes as a means of distinguishing the conservative dynamical processes from non-conservative ones.

For an incompressible fluid, the domain-integrated APE $\mathscr{E}_{ap}$ is defined as the difference between the total potential energy $\mathscr{E}_p$ and the potential energy of a reference

† Email address for correspondence: nmolem@atmos.ucla.edu

state $\mathscr{E}_p^*$,

$$\mathscr{E}_{ap} = \mathscr{E}_p - \mathscr{E}_p^* = -\int\int\int z\,(b - b^*)\,\mathrm{d}x\,\mathrm{d}y\,\mathrm{d}z, \tag{1.1}$$

where g is the gravitational acceleration acting downward in the vertical direction $\hat{\mathbf{z}}$ and $b = g(1 - \rho/\rho_0)$ is the buoyancy field proportional to the density ρ conserved on fluid parcels in the absence of diffusion or heating or material sources; ρ_0 is a background constant value, and appropriately for incompressible fluid dynamics, we have normalized all energy densities by ρ_o; $b^*(z)$ is the reference buoyancy profile that corresponds to the lowest state of potential energy that can be reached by adiabatic rearrangement of all the parcels within a bounded domain. Therefore, $N^2 = \partial_z b^* \geqslant 0$ is non-negative, and hence b^* is not unstably stratified with respect to adiabatic parcel displacements, even if $\partial_z b$ is negative in some places. The unavailable potential energy is defined by the residual,

$$\mathscr{E}_{up} = \mathscr{E}_p - \mathscr{E}_{ap}, \tag{1.2}$$

which is equivalent to $\mathscr{E}_p^*$. A stably stratified resting state has $\mathscr{E}_{ap} = 0$ and $\mathscr{E}_{up} = \mathscr{E}_p = \mathscr{E}_p^*$.

In analogy with the local KE density, $E_k = \boldsymbol{u}^2/2 \geqslant 0$ – and for conservative dynamical exchanges with it through the vertical buoyancy flux wb (§ 3) – we are interested in identifying the local APE density $E_{ap} \geqslant 0$ that is integrally consistent with (1.1),

$$\mathscr{E}_{ap} = \int\int\int E_{ap}\,\mathrm{d}x\,\mathrm{d}y\,\mathrm{d}z, \tag{1.3}$$

and that has a readily interpretable local dynamical balance equation leading to a meaningful wavenumber spectral expression analogous to that for KE. The integrand in (1.1) is not an acceptable choice for local APE density because it is not sign definite.

The dynamical approximations of small-amplitude gravity waves linearized about a stably stratified resting state and the quasi-geostrophic asymptotic limit (where buoyancy fluctuations are assumed weak compared with the background stratification) both have an energy conservation principle with a local potential energy density that satisfies our requirements for APE density, viz.

$$E_{ap} = \frac{1}{2}\frac{(b - b^*)^2}{N^2} \geqslant 0. \tag{1.4}$$

Here $b^*(z)$ is identified with the resting-state stable, time-invariant stratification (Pedlosky 1987), and the rearrangement of b is assumed to be b^*. However, this expression is not a valid E_{ap} in more general dynamical regimes with finite-amplitude differences between b and $b^*(z)$.

Several valid general expressions for the E_{ap} have been proposed (Holliday & McIntyre 1981; Henyey 1983; Shepherd 1993), inclusive of flows that are unstably stratified. They all require a determination of $b^*(z)$ by adiabatic rearrangement. An alternative approach was suggested in Tseng & Ferziger (2001), where a probability density function of b was used to approximate b^*.

A special case is the situation in which the reference-state stratification profile $b^* = N_0 z$ is linear in z with constant $N = N_0$. Equation (1.4) then provides a valid local potential energy density and $\mathscr{E}_p$ with respect to its conservative exchange with KE, even for finite-amplitude $b - b^*$ (e.g. Lindborg 2006). Whether it is a valid APE depends on whether its rearranged b profile is equivalent to $N_0 z$ and whether it is quadratic in fluctuation amplitude in the limit of small buoyancy fluctuations (Shepherd 1993). For a general $b^*(z, t) \neq N_0^2 z$, there is no valid, finite-amplitude E_{ap} form similar to (1.4).

In this paper we propose an improved technique for estimating b^* and $\mathscr{E}^*_{ap}$ for gridded data in a numerical model (§2); we adapt the E_{ap} definition of Holliday & McIntyre (1981) for a more useful local energy balance (§3) and its spectral-transform expression (§4); and we interpret the evolutionary influences on E_{ap} for some simple illustrative situations and for the rotating stratified turbulent-equilibrium state in an Eady-like vertical-shear flow (§5).

While this paper only explicitly addresses sorting procedures on a uniform grid in a uniform-depth domain, equivalent methods may be used for non-uniform grids or models with a non-trivial bottom-depth variation. There is no ambiguity in defining the reference state in any simply connected domain, since all parcels can be adiabatically rearranged in a global sorting; however, it is easy to imagine a situation with a shallow sill between two sub-basins in which the full availability of the $\mathscr{E}_{ap}$ for KE conversion is dynamically implausible (e.g. the Strait of Gibraltar between the Mediterranean and Atlantic).

The generalization of our methods to more general equations of state with compressibility is challenging. Andrews (1981) extended the E_{ap} definition of Holliday & McIntyre (1981) to a compressible fluid (inclusive of an ideal gas), obtaining an expression related to potential density, but the latter has a non-unique definition in sea water through its dependence on reference pressure (McDougall 1987). Expressions for $\mathscr{E}_{ap}$ for sea water exist (Bray & Fofonoff 1981; Reid, Elliot & Olson 1981), but we are not aware of an appropriate E_{ap} definition.

2. Estimation of the reference state

For most geophysical applications the technique proposed in Winters *et al.* (1995) is used for determining b^* in numerical simulation models. They suggest that a numerical sorting algorithm can be employed to rearrange parcels, with the densest fluid assigned to the available grid boxes that have the lowest vertical coordinate. This method allows for computation of the reference state potential energy density $E^*_p = -z\,b^*$, and therefore $\mathscr{E}_{ap}$, using (1.1).

In Molemaker, McWilliams & Capet (forthcoming), a small modification to the sorting procedure is introduced that allows for a more accurate determination of E^*_p. After sorting in three dimensions among the finite number of model grid boxes as in Winters *et al.* (1995), a resulting buoyancy field $b_s(x, y, z)$ is characterized by small departures from a horizontally uniform profile. This means that even though the potential energy $\mathscr{E}_{ps}$ of the sorted field is the lowest $\mathscr{E}_p$ that can be reached for a given grid resolution there is still some potential energy available for exchange with $\mathscr{E}_k$. We can assume that these departures are small relative to the vertical stratification of both the sorted and uniform states. In fact, the departures are guaranteed to be smaller than the difference in density between the successive vertical levels. For this sorted three-dimensional field, the linearized definition of APE (1.4) is quite accurate. We therefore propose that the APE of the sorted buoyancy field be evaluated using

$$\mathscr{E}_{aps} = \frac{(b_s - \bar{b}_s)^2}{2\partial_z \bar{b}_s}, \tag{2.1}$$

with the overbar defined as a horizontal average. The APE of the actual buoyancy field can now be calculated by the amended formula,

$$\mathscr{E}_{ap} = \mathscr{E}_p - \mathscr{E}_{ps} + \mathscr{E}_{aps}, \tag{2.2}$$

where $\mathscr{E}_{ps}$ is the potential energy of $\bar{b}_s$ and $\mathscr{E}_{aps}$ is the integral of (2.1). In discrete computations we approximate b^* by $\bar{b}_s$. Convergence tests show that the

approximation (2.2) maintains second-order accuracy with grid spacing. It is compared with other discrete $\mathscr{E}_{ap}$ estimates in § 5.1.

3. APE density and its dynamical balance equation

For definiteness consider the advection–diffusion equation for buoyancy in an incompressible fluid:

$$\frac{\mathrm{D}b}{\mathrm{D}t} = \mu \nabla^2 b, \tag{3.1}$$

where μ is the diffusion coefficient and $\mathrm{D}/\mathrm{D}t = \partial_t + \boldsymbol{u}\cdot\nabla$ is the substantial derivative. (The illustrative solutions discussed in § 5 are all based on some form of (3.1).) An appropriate local expression for E_{ap} is introduced in Holliday & McIntyre (1981) for a model in which b is a dependent variable and z is an independent variable:

$$E_{ap}(x, y, z, t) = \int_{b^*(z,t)}^{b(x,y,z,t)} \left(\mathscr{Z}[\tilde{b}] - \mathscr{Z}[b^*]\right)\, \mathrm{d}\tilde{b} \geqslant 0. \tag{3.2}$$

Here $\mathscr{Z}[b]$ is the inverse function defined by the reference state stratification $b^*(z)$. For small departures of $b(x, y, z, t)$ from $b^*(z)$, the integrand can be Taylor expanded and can be explicitly integrated to yield (1.4) with $\mathrm{d}\mathscr{Z}/\mathrm{d}b\,(b^*) = N^{-2}$. For finite-sized departures this E_{ap} formula is an appropriate evolutionary companion for E_k in a local energy conservation principle (Appendix).

Since b^* is determined from b (§ 2), $E_{ap}[b]$ is an explicit function of b alone (albeit implicitly a function of (x, y, z, t)). Therefore, we can evaluate a local balance equation for E_{ap} using the local buoyancy equation together with appropriate functional derivatives of E_{ap}. This approach is implicit in the balance equations derived in the Appendix. However, for an energy analysis of a numerical simulation, it is more accurate – and more readily generalized to more complex model dynamics than (3.1) – to take an operational approach by performing discrete operations on the discrete form of the terms in the buoyancy equation than by evaluating the derived energy-balance terms (e.g. (A 1) in the Appendix) with independent discretizations. Following the operational approach, we can formally write the local APE evolution equation as

$$\frac{\partial E_{ap}}{\partial t} = Adv\,[E_{ap}] + Dif\,[E_{ap}], \tag{3.3}$$

where Adv and Dif are the effects on E_{ap} of the advection and diffusion operators in (3.1), respectively. These operators are evaluated by finite-difference functional derivatives, e.g.

$$Adv\,[E_{ap}] = \frac{E_{ap}[b - \delta\ (\boldsymbol{u}\cdot\nabla)b] - E_{ap}[b]}{\delta}. \tag{3.4}$$

The operator E_{ap} in the numerator on the right-hand side is an evaluation of the APE using (3.2) with the indicated argument. Here, $-(\boldsymbol{u}\cdot\nabla)b$ is the local buoyancy advective-tendency operator as evaluated in the discretized numerical model; δ is chosen to be small but large enough to avoid numerical rounding errors. The simple difference in (3.4) is chosen for its efficiency of evaluation; although it is only a first-order scheme accurate in δ, the latter can be chosen to be small enough to ensure sufficient accuracy. Similarly, for a linear diffusion operator as in (3.1),

$$Dif\,[E_{ap}] = \frac{E_{ap}[b + \delta\ \mu\ \nabla^2 b] - E_{ap}[b]}{\delta}, \tag{3.5}$$

where $\nabla^2 b$ is the discrete diffusion operator and μ is the buoyancy diffusivity. If an alternative small-scale regularization operator is used in place of ∇^2 (a common practice in computational fluid dynamics as a parameterization of unresolved turbulent mixing processes), it can be evaluated analogously. The same approach can be taken for any other non-conservative (diabatic) terms in the buoyancy equation (e.g. the stratification–restoration and wavenumber-one damping terms in § 5.3).

Using these discrete approximations we can evaluate (3.3) at each point in the domain and analyse the energetic consequences of different terms in the buoyancy equation in a way that is consistent with the particular discrete operators used in the integration model for b. A spatial integration of $Adv\,[E_{ap}]$ and $Dif\,[E_{ap}]$ over the whole domain then leads to a global balance equation for $\mathscr{E}_{ap}$ and, in particular, allows the evaluation of the energy conversions with $\mathscr{E}_k$ and $\mathscr{E}_{up}$, the dissipation rate for APE and the APE boundary fluxes, if any.

4. Spectral analysis of APE balance

In the context of low-frequency, large-scale oceanic circulation, we are particularly interested in the dynamical routes towards energy dissipation on the microscales for both KE and APE (Muller, McWilliams & Molemaker 2005; Molemaker *et al*., forthcoming). For this we require a spectral analysis of (3.3) to identify the wavenumber transfer function (i.e. APE cascade). In their present form (3.2) and (3.3) are not suited for spectral analysis. In particular, the wavenumber spectrum of a term in the E_{ap} balance equation (3.3) is by definition a positive quantity; yet the individual terms can be positive or negative to increase or decrease the energy at a particular location or at a given wavenumber.

For a spectral analysis of the KE density and its balance equation, the common practice is to use its local quadratic definition, $E_k = \boldsymbol{u}^2/2 \geqslant 0$, and to operate on $\boldsymbol{u}$ and the momentum equation by multiplying their Fourier transforms by the complex conjugate of the transform of $\boldsymbol{u}$, i.e. to compute the auto-spectrum of $\boldsymbol{u}$ and the co-spectra associated with various forces. By convention the spectrum of $\boldsymbol{u}$ is called the KE spectrum, which is not the same as the spectrum (i.e. square of the magnitude of the Fourier transform) of local energy density $\boldsymbol{u}^2/2$. Since E_{ap} in (3.2) is positive semi-definite and has the units (m^2 s^{-2}) of a quadratic quantity, we introduce a new quantity $\mathscr{A}$ with units of (m s^{-1}), analogous to the role played by $\boldsymbol{u}$ in E_k:

$$E_{ap} = \frac{1}{2}\mathscr{A}^2. \tag{4.1}$$

We call $\mathscr{A}$ the gravitational disturbance field, since it is related to the amount of gravitational energy that is contained in the spatial disturbance of the density field relative to its reference state b^* (loosely analogous to the role of the displacement or extension field in the definition of elastic potential energy). In a small-fluctuation limit, E_{ap} is given by (2.1); hence $\mathscr{A} \to (b - b^*)/N$. More generally, we propose that $\mathscr{A}$ should be defined by

$$\mathscr{A} = sgn[b - b^*]\sqrt{2E_{ap}}. \tag{4.2}$$

With this definition we can rewrite (3.3) as

$$\mathscr{A}\frac{\partial \mathscr{A}}{\partial t} = \mathscr{A}\ Adv\,[\mathscr{A}] + \mathscr{A}\ Dif\,[\mathscr{A}], \tag{4.3}$$

where $Adv\,[\mathscr{A}]$ and $Dif\,[\mathscr{A}]$ are calculated analogous to (3.4) and (3.5) (i.e. the functional derivative now is taken on $\mathscr{A}$ rather than for E_{ap}).

An APE spectrum is then obtained as the power spectrum of $\mathscr{A}$,

$$E_{ap}(k) = \frac{1}{2}\,[\hat{\mathscr{A}}(k)]^{+}\,\hat{\mathscr{A}}(k), \tag{4.4}$$

with $\hat{\mathscr{A}}(k)$ the Fourier transform of $\mathscr{A}(x, y, z)$ and $[\cdot]^{+}$ the complex conjugate. Spectral versions of the different terms in the energy balance (4.3) are analogously obtained using co-spectra of $\hat{\mathscr{A}}(k)$ and the transformed right-hand side terms.

Thus, a simple quadratic factorization of the $E_{ap} \geqslant 0$ definition by Holliday & McIntyre (1981) yields an evolutionary equation of $\mathscr{A}$ that can be manipulated to provide a spectrally decomposed APE balance. As shown by the examples in § 5 the terms in the $\mathscr{A}$ equation are functionally well behaved in spite of its derivation through division by $\mathscr{A}$. An analogous approach could be taken to other valid E_{ap} definitions that might be more suitable for models expressed in different dependent and independent variables (e.g. Henyey 1983; Shepherd 1993).

5. Applications

In this section we present three examples of the spatial structure and evolutionary behaviour of E_{ap} and its dynamical balance equation. The first example is a tilted, stratified buoyancy field that spins down to a resting state. This example is used to compute $\mathscr{E}_{ap}$ in several different ways to assess their accuracy. The second example is an unstable stratification that evolves passively in a specified overturning circulation. The third example is an application of our APE methodology to complete the energetics analysis of the turbulent-equilibrium Eady flow otherwise examined in Molemaker *et al.* (forthcoming).

5.1. *Spin-down of a tilted buoyancy field*

Consider the following non-rotating non-hydrostatic non-dimensional quasi-linear Boussinesq fluid system:

$$\begin{aligned} \partial_t \boldsymbol{u} &= -\nabla\phi + \hat{\boldsymbol{z}}b + \nabla^2\boldsymbol{u}, \\ \nabla\cdot\boldsymbol{u} &= 0, \\ \partial_t b &= -\nabla\cdot(\boldsymbol{u}b), \end{aligned} \tag{5.1}$$

where $\boldsymbol{u}$ is a velocity vector (u, v, w); b is the buoyancy; and ϕ is the normalized pressure anomaly p/ρ_0. The domain is $x \in [0, 1] \times y \in [0, 1] \times z \in [0, 1]$, and the boundary conditions are no normal flow and no flux of momentum. This system is adiabatic, since the buoyancy equation does not include a diffusive term. We define initial values for the fields $(\boldsymbol{u}, b, \phi)$ with $\boldsymbol{u} = 0$, $b(x, y, z) \neq 0$ a tilted, stably stratified buoyancy field and ϕ in hydrostatic balance with b. Starting from this motionless state, flow develops in the (x, z) plane through gravitational acceleration and sloshing. This creates a non-zero value for $\mathscr{E}_k$ by buoyancy-flux conversion (release) of potential energy. The $\mathscr{E}_k$ is subsequently dissipated by viscous diffusion, which is thus a route to dissipation for the initial-state $\mathscr{E}_{ap}$. The end of this evolution is a return to a horizontally uniform resting state as $t \to \infty$, where the buoyancy field corresponds to b^*, the state with the lowest potential energy that can be reached adiabatically.

As a particular case consider an initial buoyancy field with a uniform, tilted spatial gradient:

$$b(x, y, z, 0) = \gamma(z - 0.5) + \alpha(x - 0.5). \tag{5.2}$$

Resolution	Sorting	Fine sorting	Amended sorting (2.2)	Local definition (3.2)
16×16	0.2526×10^{-3}	-0.1554×10^{-3}	0.0391×10^{-3}	0.0300×10^{-3}
32×32	0.0666×10^{-3}	-0.0390×10^{-3}	0.0117×10^{-3}	0.0100×10^{-3}
64×64	0.0174×10^{-3}	-0.0098×10^{-3}	0.0033×10^{-3}	0.0030×10^{-3}
128×128	0.0044×10^{-3}	-0.0024×10^{-3}	0.0009×10^{-3}	0.0008×10^{-3}
256×256	0.0011×10^{-3}	-0.0006×10^{-3}	0.0002×10^{-3}	0.0002×10^{-3}

TABLE 1. Discrete convergence behaviour for the error in $\mathscr{E}_{ap}$ as a function of spatial resolution for different definitions of $\mathscr{E}_{ap}$ in the tilted-stratification example with $\alpha = 0.4$ and $\gamma = 1$. The truth standard is the analytic value $\mathscr{E}_{ap} = 6.133 \times 10^{-3}$, and the error for the weak-fluctuation definition (1.4) analytic value is $\mathscr{E} = 0.533 \times 10^{-3}$. The recommended new techniques are in the last two columns on the right.

If $|\alpha| < \gamma$, the stratification is gravitationally stable everywhere; $\alpha \ll \gamma$ is the weak-fluctuation limit.

For system (5.1) the potential energy $\mathscr{E}_p$ is calculated as

$$\mathscr{E}_p = -\int\int\int z\ b\ \mathrm{d}b = \gamma \left(\frac{1}{3} z^3 - \frac{1}{4} z^2 \right) \Big|_0^1 = \frac{1}{12} \gamma, \tag{5.3}$$

and the APE is

$$\mathscr{E}_{ap} = \frac{\alpha^2}{24\gamma} - \frac{\alpha^3}{120\gamma^2}. \tag{5.4}$$

This reduces to the weak-fluctuation expression $E_{ap} = \alpha^2 / 24\gamma$ for $\alpha \ll \gamma$.

In figure 1 E_{ap} is shown for different values of α for a configuration with a 16×16 grid. This is a rather coarse grid resolution, but it is chosen to highlight differences between different numerical approximations of E_{ap}; furthermore, the use of relatively few vertical levels is common in atmospheric and oceanic modelling. The comparison standard is (5.4). The method of sorting on the three-dimensional model grid (Winters *et al.* 1995) (blue line in figure 1) is noticeably inaccurate even for small values of α/γ, and it consistently underestimates $\mathscr{E}_{ap}$ by neglecting the residual $\mathscr{E}_{ap}$ that remains after the sort. The alternative with a much finer vertical grid (yellow line in figure 1) – essentially giving each individual three-dimensional grid cell its own vertical level – consistently leads to an overestimation of $\mathscr{E}_{ap}$. This results from the difference in the number of vertical levels used for the reference $\mathscr{E}_p$ and the current $\mathscr{E}_p$. The weak-fluctuation formula departs from the finite-amplitude formula quadratically in α/γ (magenta line in figure 1). The new discrete methods (red and green lines in figure 1) provide substantially more accurate approximations to the alternatives over a large α/γ range. Table 1 shows convergence behaviour for all four methods. Shown in the table are the errors for the different methods relative to the analytical value of $\mathscr{E}_{ap}$ for increasing resolution. From the table, it can be seen that all methods converge to the analytical value at a rate that is second order in grid resolution. However, the methods suggested in this paper provide the smallest errors for any given grid resolution.

Figure 2 shows the results of the time integration with a discretized form of the set of equations (5.1). A second-order, central-difference scheme is used to advect the buoyancy field, since it is strictly non-dissipative. Temporal-integration errors are minimized by using a second-order Adams–Bashforth time-stepping algorithm with very small time steps. The system is integrated in time until a resting state occurs.

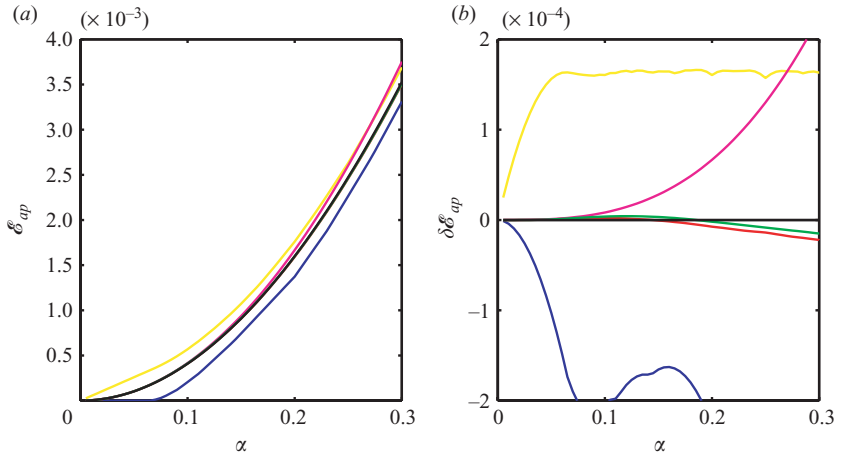

FIGURE 1. The $\mathscr{E}_{ap}$ for the tilted stratification example for a range of α values and $\gamma = 1$: (a) includes the analytically computed value (5.4) (black line), the analytic weak-fluctuation value (1.4) (magenta line), the value found by sorting on the model grid (blue line), the value found by redistribution and computation of $\mathscr{E}_{ps}$ with a 16-time finer vertical grid (yellow line), the amended sorting technique (2.2) (red line) and the domain integral of the local definition of E_{ap} (3.2) (green line); (b) replots the same curves as the differences $\delta\mathscr{E}_{ap}$ from the analytically computed $\mathscr{E}_{ap}$ (5.4). The recommended new techniques are the red and green lines.

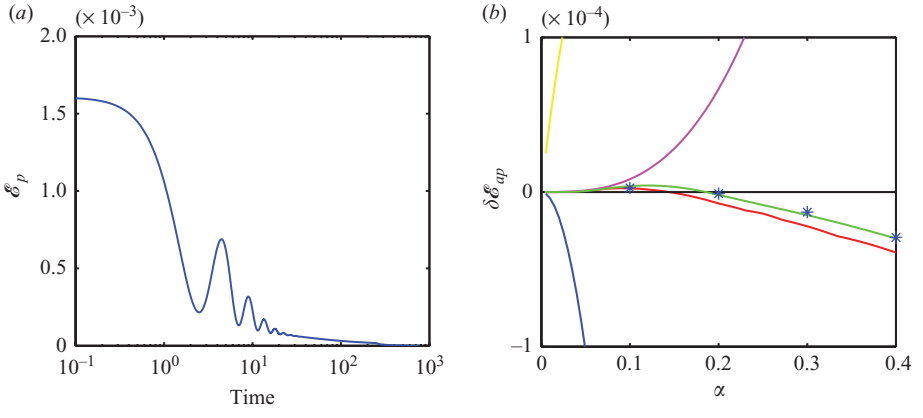

FIGURE 2. Spin-down of the tilted stratification in (5.2): (a) shows the potential energy relative to the final value as a function of time until the system is at rest. The difference between initial and final $\mathscr{E}_p$ values is the discrete $\mathscr{E}_{ap}$; (b) is a blow-up of figure 1(b) but adds the results of the time integration of the discrete system as blue symbols for comparison with the initial-state estimates of $\delta\mathscr{E}_{ap}$.

Figure 2(a) shows the evolution of $\mathscr{E}_p$. Initially the system is at rest. For $t > 0$, $\mathscr{E}_{ap}$ is converted into $\mathscr{E}_k$, which is subsequently dissipated by viscosity. When the $\mathscr{E}_p$ of the system is at the lowest possible value, there is no more $\mathscr{E}_p$ available for conversion, and the system returns to rest. The $\mathscr{E}_{ap}$ of the original state is equal to the difference between the E_p values in the initial and final states. Oscillations in the evolution of $\mathscr{E}_p$ indicate back-and-forth exchanges between KE and APE. Figure 2(b) is a copy of figure 1(b) with late-time integration results added (asterisks). The reduction of $\mathscr{E}_{ap}$ realized in the spin-down simulation agrees quite well with the initial estimates

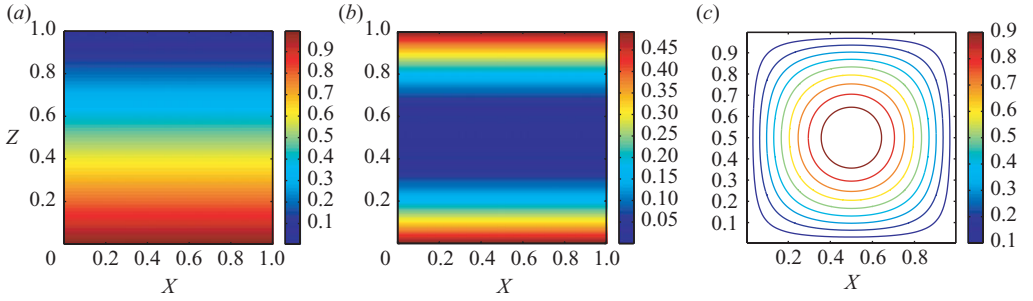

FIGURE 3. Initial state for b, E_{ap} and Ψ in the stratified overturning example.

by the new procedures, and they are nearly indistinguishable in this example. They agree even better with each other than the analytically computed initial value, which indicates the mutual consistency between the discrete $\mathscr{E}_{ap}$ estimates and the discrete model evolution.

In this adiabatic example there is no exchange between $\mathscr{E}_{ap}$ and $\mathscr{E}_{up}$. Initially the total potential energy of the buoyancy field is $\mathscr{E}_p = \mathscr{E}_{up} + \mathscr{E}_{ap}$. For $t \to \infty$ all $\mathscr{E}_{ap}$ has been converted into $\mathscr{E}_k$ and subsequently dissipated, reducing $\mathscr{E}_p$ by exactly that amount. Therefore, throughout the evolution $\mathscr{E}_{up}$ does not change.

5.2. *Unstably stratified overturning flow*

In this section we present an illustrative example of the local quantities in the new algorithm for E_{ap} and its evolution. The initial condition is the unstably stratified buoyancy field,

$$b(x, z, 0) = 1 - z \tag{5.5}$$

in a two-dimensional domain ($x \in [0, 1]$, $z \in [0, 1]$) with no buoyancy flux through the boundary. This buoyancy field evolves by the advection–diffusion equation,

$$\frac{\partial b}{\partial t} = -(\boldsymbol{u} \cdot \nabla) b + \mu \nabla^2 b, \tag{5.6}$$

where the two-dimensional, non-divergent velocity $\boldsymbol{u} = (u, 0, w)$ is prescribed as constant in time with $u = -\partial_z \Psi$, $w = \partial_x \Psi$ and a stream function specified by

$$\Psi(x, z) = \sin[\pi x]\, \sin[\pi z]. \tag{5.7}$$

The diffusion coefficient is set to the relatively small value of $\mu = 2 \times 10^{-3}$. Figure 3 shows the initial b, E_{ap} and Ψ fields; E_{ap} has its maximum values near the upper and lower boundaries showing the largest difference between the local b and b^*.

Equation (5.6) is integrated numerically in time to a fraction of the turnover time for the circulation, $t = 0.5$. The resulting b, E_{ap} and $\mathscr{A}$ are shown in figure 4. The buoyancy field is being swept around by the circulation. As a result of advection by the steady velocity field, some of the higher buoyancy values are transported upwards, and the lower ones are transported downwards, reducing both $\mathscr{E}_p$ and $\mathscr{E}_{ap}$. In addition to a reduction of $\mathscr{E}_{ap}$ in the integral sense, the E_{ap} field has been rearranged as well. Figure 4(c) shows the spatial distribution of $\mathscr{A}$. While it has a gross similarity to b, the field of $\mathscr{A}$ in (4.2) is quantitatively rather different, consistent with the definition of E_{ap} in (3.2).

Figure 5 shows the E_{ap} tendency patterns that result from the advection of b in (5.6) in the unstably stratified example. Figure 5(a) shows advection of b, which heats the upper-left corner of the domain and cools the lower-right corner, thus reducing

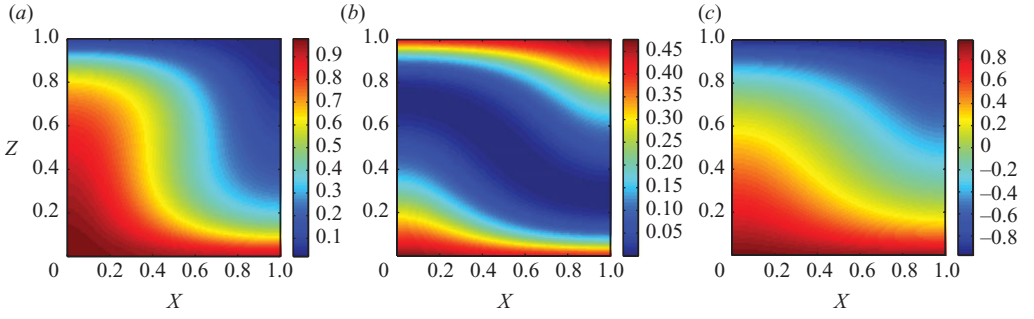

FIGURE 4. Fields of (*a*) b, (*b*) E_{ap} (*c*) and $\mathscr{A}$ at $t=0.5$ for the stratified overturning example (figure 3) evolving through advection and diffusion in (5.6).

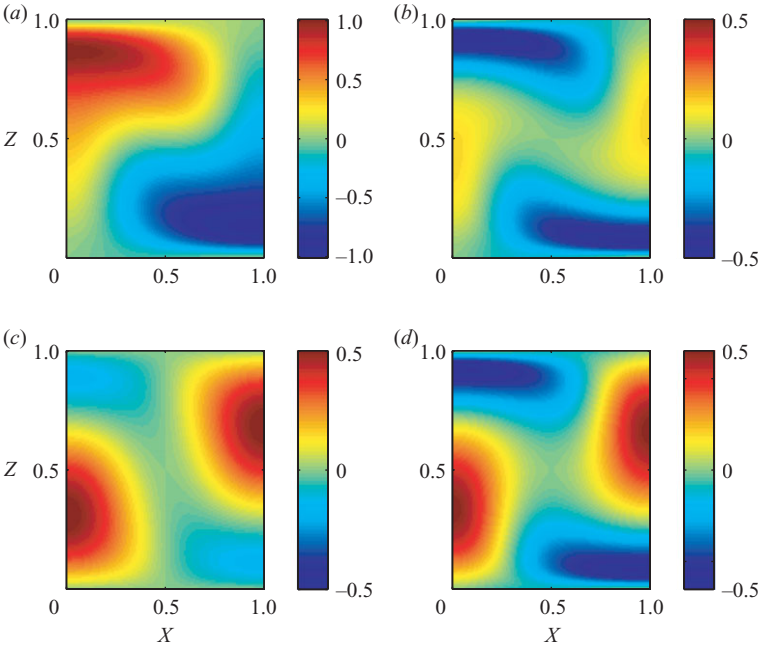

FIGURE 5. Spatial pattern of tendencies that result from the advection of b for the stratified overturning example in figure 3 at $t=0.5$: (*a*) $-(\boldsymbol{u}\cdot\nabla)b$; (*b*) $Adv[E_{ap}]$; (*a*) $w(b-b^*)$; and (*d*) $-(\boldsymbol{u}\cdot\nabla)E_{ap}$. The advective evolution of E_{ap} is a combination of redistribution of E_{ap} by $\boldsymbol{u}\cdot\nabla E_{ap}$ and conversion of potential energy by $w(b-b^*)$.

E_{ap} overall. Figure 5(*b*) shows the effect of $\boldsymbol{u}\cdot\nabla b$ on the distribution of E_{ap}. This pattern is not a pure redistribution of E_{ap} because it also reflects the reduction of $\mathscr{E}_{ap}$ by conversion to $\mathscr{E}_k$. The pattern of $Adv[E_{ap}]$ is the combination of $(\boldsymbol{u}\cdot\nabla)E_{ap}$, a pure spatial redistribution of E_{ap} by the overturning circulation, and w $(b-b^*)$, the buoyancy-flux conversion of E_{ap} into E_k with extrema in the regions of strong vertical motion and large deviation of b from the reference profile. These results illustrate how the distribution of that E_{ap} and its local tendency influences are not merely mathematical constructs but in fact have a mechanistically interpretable meaning.

Shifting attention to the gravitational disturbance field $\mathscr{A}$, the upper row of figure 6 compares the advection of b, $-(\boldsymbol{u}\cdot\nabla)b$, with the advective influence on $\mathscr{A}$, $Adv[\mathscr{A}]$,

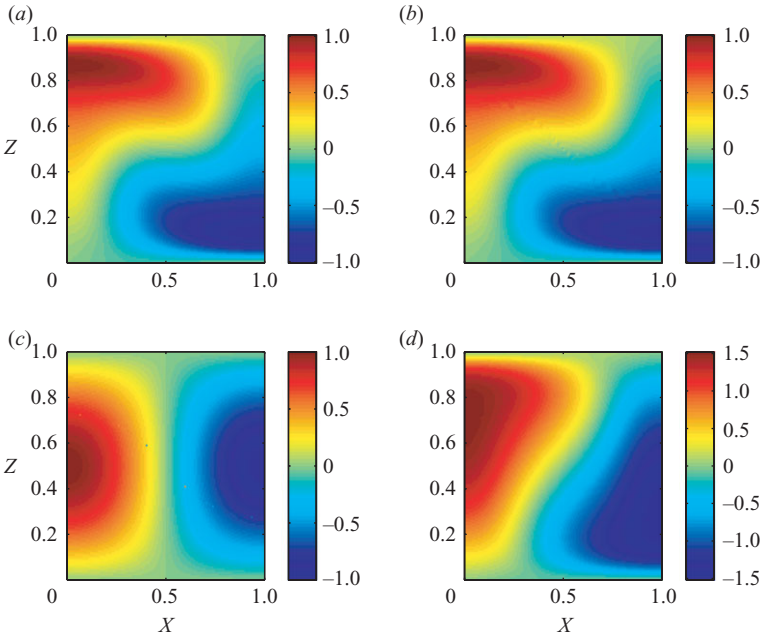

FIGURE 6. Spatial pattern of tendencies from the advection of b for the stratified overturning flow at $t = 0.5$: (*a*) $-(\boldsymbol{u}\cdot\nabla)b$; (*b*) $Adv[\mathscr{A}]$; (*c*) $-w(b-b^*)/\mathscr{A}$; and (*d*) $-(\boldsymbol{u}\cdot\nabla)\mathscr{A}$. The effect of advection on $\mathscr{A}$, $Adv[\mathscr{A}]$, is the sum of $w(b-b^*)/\mathscr{A}$ and $-(\boldsymbol{u}\cdot\nabla)\mathscr{A}$ to within the second-order accuracy of the discretizations.

demonstrating their close correspondence for this case. Unlike the relations among $Adv[E_{ap}]$, $w(b-b^*)$ and $-(\boldsymbol{u}\cdot\nabla)E_{ap}$, the former correspondence is not exact in all cases. The lower row of figure 6 shows $w(b-b^*)/f$ and $-(\boldsymbol{u}\cdot\nabla)\mathscr{A}$, which added together lead to the pattern of $Adv[\mathscr{A}]$.

Further examination of the results shows that

$$Adv[E_{ap}] + w(b-b^*) = -(\boldsymbol{u}\cdot\nabla)E_{ap} \tag{5.8}$$

within the second-order numerical accuracy of the discretizations used to approximate (3.2). Furthermore, we find that

$$Adv[\mathscr{A}] - w(b-b^*)/\mathscr{A} = -\boldsymbol{u}\cdot\nabla\mathscr{A}, \tag{5.9}$$

which follows from the equivalent relation for the advection of E_{ap} and the definition of $\mathscr{A}$ in (4.2).

The diffusive term in (5.6) and its effect on $\mathscr{A}$ are now examined. Again, the evolution of $\mathscr{A}$ as a result of $\nabla^2 b$ appears to be closely related to $\nabla^2 b$ itself. The effect of diffusion on E_{ap} is given by $\mathscr{A}\ Dif[\mathscr{A}]$, and for this case it is negative when integrated over the domain, dominated by regions of E_{ap} destruction near the upper and lower boundaries. These regions are characterized by larger values of both $|\nabla^2 b|$ and E_{ap}. An expression for the effect of diffusion of b on the evolution of E_{ap} is derived in the Appendix (see (A 1)). The diffusive term in (A1) are not very straightforward, and diffusion is not strictly a sink of E_{ap} in all situations (see figure 7).

5.3. *Spectral energy balance in an equilibrium Eady flow*

Molemaker *et al.* (forthcoming) analyzed the turbulent-equilibrium state of an unstable geostrophically balanced vertically sheared horizontal flow with uniform

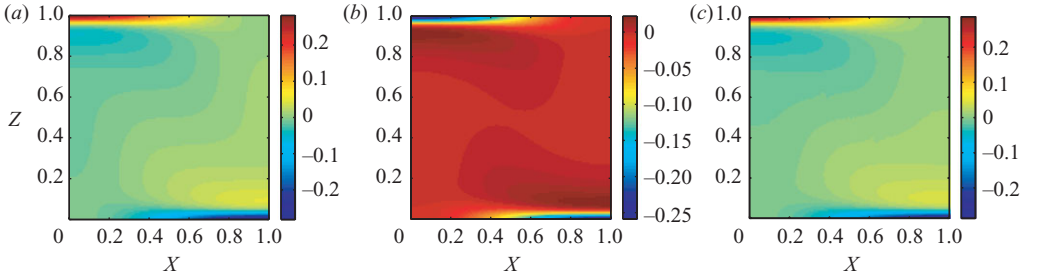

FIGURE 7. Spatial pattern of tendencies that result from the diffusion of b for the stratified overturning example in figure 3 at $t = 0.5$: (*a*) $\mu\nabla^2 b$, (*b*) $Dif\,[E_{ap}]$ and (*c*)$Dif\,[\mathscr{A}]$.

background rotation and stable stratification in a horizontally periodic, vertically bounded domain for solutions of the non-dimensional incompressible rotating non-hydrostatic Boussinesq equations with viscosity and diffusion. This is the mean flow analysed by Eady (1949) for its quasi-geostrophic linear baroclinic instability and for more general linear instabilities by Stone (1966) and Molemaker, McWilliams & Yavneh (2005). In the turbulent-equilibrium solution the unstable mean flow is maintained by artificial restoration towards uniform shear and stratification, and the fluctuations are artificially damped at the domain scale (to absorb an inverse energy cascade); the associated rate constants are chosen to be small enough to not overwhelm the advective fluid dynamics. The Rossby and Froude numbers based on the mean shear flow are chosen to be equal to 0.5, which is small enough so that the dynamical effects of rotation and stable stratification are important but large enough so that ageostrophic currents emerge clearly. The first baroclinic deformation radius is chosen as $L_r = 0.1$ in a domain with a domain width $L = 1$. The Reynolds number is as large as computationally feasible.

The fluctuations about the Eady flow during the equilibrium state are a combination of the following phenomena:

(*a*) Geostrophically balanced eddies arising from instability of the mean Eady flow, with a horizontal scale near L_r and significant inverse energy cascade towards larger scales (as expected in geostrophic turbulence; Charney 1971).

(*b*) Boundary-intensified buoyancy fronts generated through straining by the larger eddies, which induce significant buoyancy restratification and generate E_k on intermediate scales by $\overline{w'b'} > 0$ conversion, with strong local deviations from geostrophic, hydrostatic balance.

(*c*) Similarly unbalanced, horizontal-shear instabilities of the fronts that arrest the frontogenesis at an intermediate scale and further advance the forward KE cascade towards small-scale dissipation.

In Molemaker *et al.* (forthcoming) particular attention is given to the energy balance in the turbulent-equilibrium state and the dynamical route to small-scale, viscous dissipation of KE. Using a modification of the sorting procedure by Winters *et al.* (1995) described in § 2, a domain-integrated $\mathscr{E}_{ap}$ balance is included in the energy analysis, along with a detailed spectral decomposition of E_k and its dynamical balance. However, a spectral analysis of E_{ap} analogous to E_k is absent. With the formulas in §§ 3 and 4, we can now complete this analysis and present a complete view of the total energy as it moves from the mean Eady flow into the eddy and frontal fluctuations, from fluctuation APE to KE and among different spatial scales in the fluctuation fields.

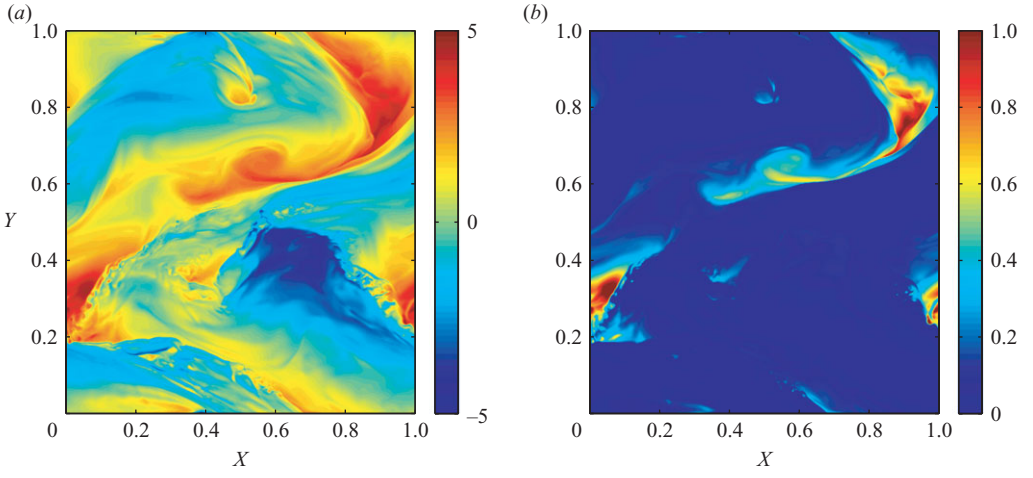

FIGURE 8. Instantaneous horizontal slices at $z = 0.9$ (in a domain with $z \in [0, 1]$) for (a) fluctuation buoyancy and (b) E_{ap} from (3.2) in an equilibrium Eady flow. Both fields are non-dimensional as described in Molemaker *et al.* (forthcoming) for the case with the Rossby number $Ro_r = V_0/fL_r = 0.5$ and the Reynolds number $Re_{eff} = V_0 L/\nu_h = 6600$ (with V_0 the vertical velocity difference in the Eady flow, L the horizontal domain size and ν_h the effective horizontal viscosity including the effect of numerical diffusion in the advection operator). The deformation radius is $L_r = 0.1$.

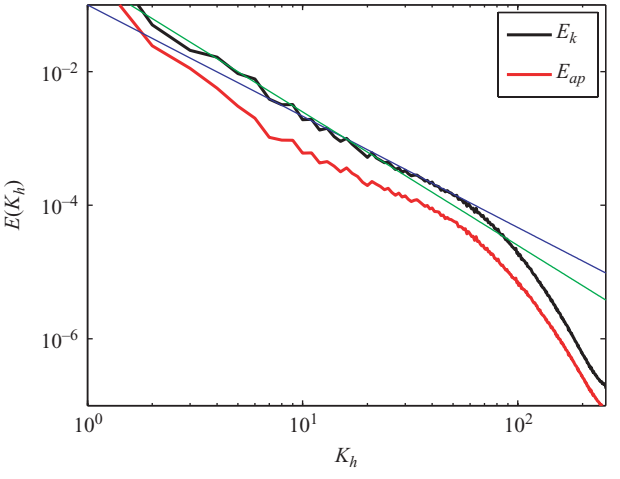

FIGURE 9. Depth-averaged horizontal-wavenumber spectra for E_{ap} (red line) and E_k (black line) associated with the $\mathscr{A}$ and $\boldsymbol{u}$ fields in an equilibrium Eady flow. The blue and green lines indicate $k^{-5/3}$ and k^{-2} power-law shapes.

Figure 8 shows horizontal planes of buoyancy fluctuation and E_{ap}. The eddies are evident on the larger scale. Intermediate-scale buoyancy fronts occur between the eddy centres. Some of the fronts also exhibit fine-scale instability. The largest values of E_{ap} are associated with positive buoyancy extrema in this plane located near the vertical boundary.

Figure 9 shows the horizontal-wavenumber ($K_h = \sqrt{k_x^2 + k_y^2}$) spectra of KE and APE, averaged in depth and time during the equilibrium phase. For all wavenumbers

E_k is larger than E_{ap} (note that the integral values are $\mathscr{E}_k = 1.40$ and $\mathscr{E}_{ap} = 0.65$), but the spectral shapes are essentially identical. Our provisional interpretation is that the overall energy ratio is set by the larger-scale (low-wavenumber) eddy dynamics, which surely does not exhibit an universal behaviour. Homogeneous geostrophic turbulence (which this is not) has a KE/APE ratio of 2 (Charney 1971), and geostrophic turbulence in a vertically bounded domain with larger horizontal extent but the same baroclinic deformation radius L_r would have a much larger APE/KE ratio. The approximate power-law shapes for the intermediate-wavenumber range $K_h \in [15, 70]$ are suggestively close to an energy inertial-cascade range exponent of $-5/3$, albeit with some imprecision owing to the limited grid resolution of the simulation (512×512 horizontally). It has proved difficult to realize an exact inertial range in spectrum shape and spectral flux in computational simulations even in the classical isotropic, homogeneous problem and even with quite high resolution (Kaneda *et al.* 2003) but in general at even higher wavenumbers, of course, the energy spectra steepen because of viscous and diffusive dissipations.

At larger scales (i.e. in the geostrophic and frontogenetic dynamical regimes; Molemaker *et al.*, forthcoming), as well as in the small-scale dissipation range, the spectrum slopes are steeper. In particular, on scales smaller than the first baroclinic deformation radius at $L_r = 0.1$ (i.e. $K_{hr} = 1.6$), we see a slope consistent with the K_h^{-2} submesoscale frontogenesis regime in Capet *et al.* (2008*a*), although its wavenumber range is rather short in the Eady problem as posed here. From this perspective we interpret the onset of the $K_h^{-5/3}$ range around $K_h = 20$ as the high-wavenumber end of the frontogenesis range in which frontal instability becomes the dominant process for further forward energy cascade.

Figure 10 (top row) shows the spectral balance of fluctuation KE E_k. At low wavenumbers a large conversion of energy from potential to KE $\overline{w'b'}$ occurs in association with larger-scale baroclinic instability of the mean Eady flow and finer-scale frontogenesis. This energy is transferred in wavenumber space by advection both to the lowest available wavenumber ($K_h = 1$, where a linear damping term is active) and to higher wavenumbers *en route* to viscous dissipation. For horizontal wavenumbers greater than $K_h \approx 15$, the buoyancy-flux conversion of E_{ap} strongly decreases, and the primary energy balance is between advective energy transfer among wavenumbers and dissipation. Since the dissipation is concentrated at the highest wavenumbers, the advective transfer rate is small for the intermediate scales because of approximately constant energy fluxes (5.10) towards the dissipation range. A constant-energy-flux range is commonly referred to as an energy inertial-cascade range (figures 9 and 11). However, in the expanded ordinate range (figure 10, upper-right panel), we see a weak, negative energy conversion from E_k to E_{ap} that modifies the simple Kolmogorov concept of a purely KE inertial-cascade range. The negative sign of this conversion from E_k to E_{ap} is reminiscent of the forward energy cascades in stratified turbulence measured at the microscale in the oceanic interior (Toole 1998), where rotational influences are presumed negligible. Within this coupled inertial range the transfer function is positive for E_k, since it balances losses because of both dissipation and negative buoyancy-flux conversion.

The bottom row in figure 10 shows the corresponding balance for E_{ap}. It has direct fluctuation generation by the instability of the mean Eady flow; E_{ap} loss by conversion mirrors the equal-but-opposite gain in the E_k balance – a positive conversion in the baroclinic instability and frontogenetic wavenumber ranges and a negative conversion in the nearly inertial range. The advective spectral transfer function for E_{ap} is more extensively positive than it is for E_k, beginning at lower

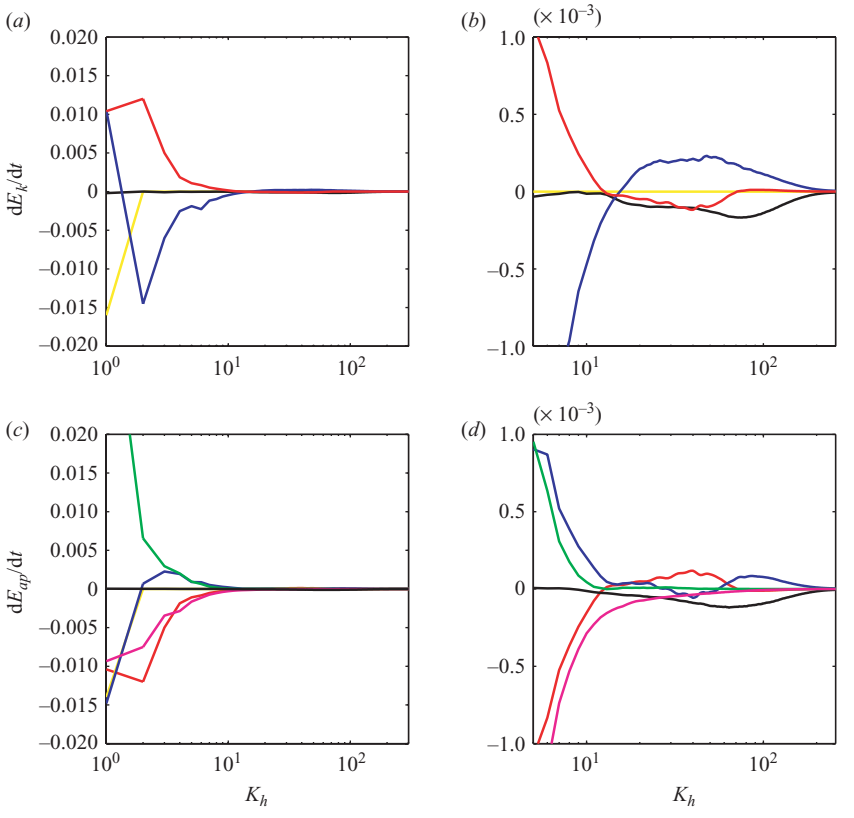

FIGURE 10. Time-averaged, horizontal spectral energy balances for the fluctuation fields in an equilibrium Eady flow. The right panels show an expanded ordinate range zooming in on the higher wavenumbers. KE balance E_k (top row): conversion of potential energy $\overline{w'b'}$ (red line); transfer function for advective E_k redistribution among wavenumbers (blue line); E_k dissipation (black line); restoration damping of wavenumber $K_h = 1$ in $\boldsymbol{u}$ (yellow line). APE balance E_{ap} (bottom row): loss of potential energy by conversion $-\overline{w'b'}$ (red line); transfer function for advective E_{ap} redistribution among wavenumbers (blue line); E_{ap} dissipation (black line); generation of fluctuations by instability of the mean Eady flow (green line); restoration of buoyancy fluctuations to the reference state stratification (maroon line); restoration damping of wavenumber $K_h = 1$ in b (yellow line). In both balances the dissipation is due to a combination of explicit diffusion and numerical dissipation associated with the third-order, upwind-biased advection scheme.

wavenumbers in association with baroclinic instability and frontogenesis. It shows negative values (suggestive of inverse cascade; see also figure 11) at the largest scales, but for intermediate wavenumbers the E_{ap} transfer function is positive in association with frontogenesis (*cf.,* Capet *et al.* 2008*b*). However, in the inertial range for $K_h > 15$ the transfer function is small, as the negative buoyancy-flux conversion (which appears as a positive term in the E_{ap} balance) balances the dissipation. At the highest wavenumbers ($K_h > 70$), the negative conversion abates, and an advective transfer function balances further dissipation.

An examination of the spectra of the terms in the vertical momentum balance shows that the gravitational force $\hat{\boldsymbol{z}}b$ contributes significantly to the dynamical balance of the fluctuations throughout the energy inertial-cascade range up to the onset of the dissipation range. This further indicates (in addition to the negative

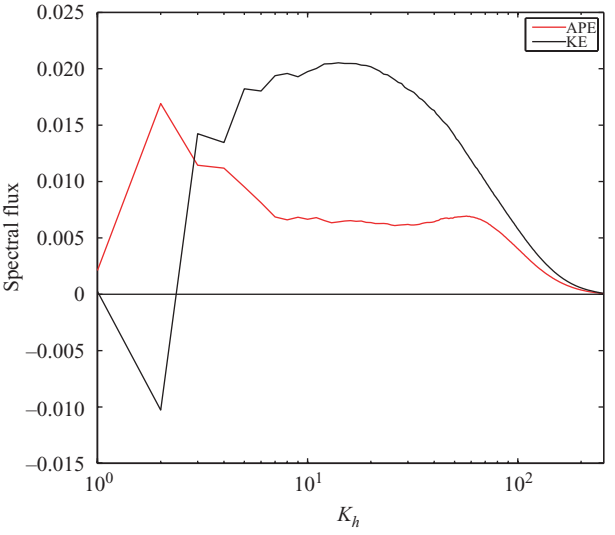

FIGURE 11. Advective spectral fluxes Π_k (black line) and Π_{ap} (red line) as functions of horizontal wavenumber in an equilibrium Eady flow. Positive values indicate forward energy cascades towards larger wavenumber. Note the approximately constant flux values for the intermediate-K_h range, especially for Π_{ap}.

conversion throughout this range) that the advective forward cascades in E_k and E_{ap} are dynamically coupled with each other.

The spectral fluxes of of E_k and E_{ap} in figure 11 are obtained by integrating the advective transfer functions in horizontal wavenumber K_h space:

$$\Pi_k(K_h) = \int_0^{K_h} Adv\,[E_k]\ \mathrm{d}K_h,$$
$$\Pi_{ap}(K_h) = \int_0^{K_h} (Adv\,[E_{ap}] + [\hat{w}]^+\hat{b})\ \mathrm{d}K_h. \tag{5.10}$$

Figure 11 clearly shows forward fluxes for both E_k and E_{ap} at most K_h, including forward flux even at the domain scale for E_{ap} (though inverse flux for E_k there). The magnitude of the forward flux is larger for E_k than for E_{ap}, reflecting the fact that there is more overall $\mathscr{E}_k$ than $\mathscr{E}_{ap}$ in the fluctuations on the intermediate scales. Consistent with figure 10, the forward flux of E_{ap} shows a rather flat curve for Π_{ap} between wavenumbers 10 and 70, consistent with an inertial-cascade range. The Π_k is not quite as flat over this range, although its variations are only around 10 %; its decrease towards the dissipation range starts are smaller values K_h than for Π_{ap} because of their dissipation curves in figure 10).

A similar forward-flux, inertial-cascade range in both E_k and E_{ap} is shown in Lindborg (2006) and Lindborg & Brethouwer (2007) for randomly forced non-rotating stratified turbulence (with a uniform background stratification N_0 posed so that the $\mathscr{E}_p$ is also an $\mathscr{E}_{ap}$); it spans a somewhat larger wavenumber range than here. Within this range it has approximately the same E_k/E_{ap} ratio as here, the same $-5/3$ spectrum power-law exponents, an extensive negative buoyancy-flux conversion (i.e. from E_k to E_{ap}) and a nearly constant spectral flux $\Pi(K_h)$ for E_{ap} compared with a modestly decreasing one for E_k. This suggests there may be a simple phenomenological

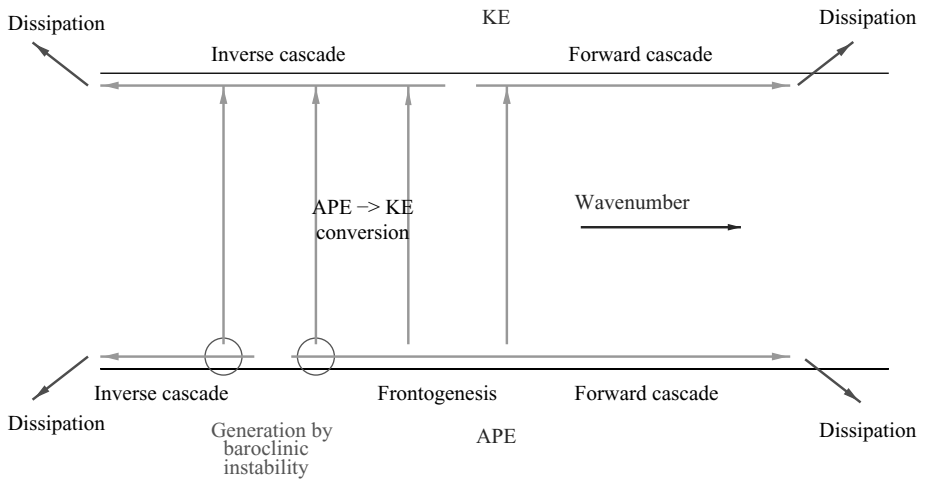

FIGURE 12. Sketch of energy pathways in an equilibrium Eady flow. Dissipation is depicted as important only at large and small scales; the former is conceived of as a 'Rayleigh' process in which the dissipation rate is proportional to spectrum amplitude that peaks at large scale and the latter as a 'Newtonian' process in which it peaks at small scale. The negative buoyancy-flux conversion in the coupled forward-cascade range is not included because of uncertainty about its asymptotic behaviour as $Re \to \infty$.

continuity in the turbulent cascades, as the rotational dynamical control decreases with increasing k in a $\sim k^{-5/3}$ spectrum range. However, to demonstrate this transition in simulations would require a broader range of resolved scales than has yet been achieved. In our simulation the rotational influence remains dynamically significant for all resolved scales. Furthermore, Riley & Lindborg (2008) interprets a variety of atmospheric and oceanic measurements as consistent with the stratified (and perhaps in some cases rotationally influenced) inertial-cascade range.

The derivation of a spatially local, spectrally decomposable E_{ap} balance (§§ 1–4 and the Appendix) cannot be extended to E_p and hence not to the residual quantity E_{up}. Nevertheless, all of the forms of potential energy have well-defined integral balances that we will now summarize for completeness. Consistent with the lower row in figure 10, the integral balance for $\mathscr{E}_{ap}$ consists of a source by mean flow instability (at a mean rate of +0.15 in the non-dimensional units used in figure 6 of Molemaker *et al.*, forthcoming), balanced by buoyancy-flux conversion to KE (−0.06), mean restratification (−0.06), $K_h = 1$ restoration (−0.02) and diffusive dissipation (−0.01). The integral balance for $\mathscr{E}_p$ is mainly loss by restratification (−0.06) and gain by restoration to the mean buoyancy profile (+0.06), with only a very weak source from vertical diffusion (+0.003); it has no direct energy exchange with $\mathscr{E}_k$ through the instability of the mean Eady flow. Thus, the integral balance for $\mathscr{E}_{up}$, determined by residual between $\mathscr{E}_p$ and $\mathscr{E}_{ap}$ balances, is gain by restoration (+0.12), loss by mean instability (−0.15) and gains by $K_h = 1$ restoration and diffusion (+0.02 and +0.01), with no contribution from buoyancy-flux conversion. Finally, the $\mathscr{E}_k$ balance (figure 6 of Molemaker *et al.*, forthcoming) is a gain from conversion of potential energy (+0.057) and losses by $K_h = 1$ restoration and fine-scale dissipation (−0.03 and −0.03, respectively).

On the basis of the spectral energy balances in figure 10, a summary diagram for the pathways for fluctuation energy from large-scale E_{ap} generation by mean-flow instability to fine-scale diffusive dissipation (and $K_h = 1$ restoration damping) is presented in figure 12. From our simulations with a finite Reynolds number and

grid resolution, we feel confident about the asymptotic validity of the coupled forward-cascade inertial range in E_k and E_{ap}, although we remain agnostic about whether the negative buoyancy-flux conversion in this range would continue indefinitely in K_h as $Re \to \infty$.

6. Summary

We have introduced two new techniques for calculating gravitational APE. The first technique (§2) is a simple modification of the volumetric buoyancy sorting procedure in Winters *et al.* (1995); it allows for a much more accurate evaluation of the domain-integrated APE in discretized numerical models. It takes advantage of the fact that while the weak-fluctuation approximation for $\mathscr{E}_{ap}$ in (1.4) may not be accurate for the actual buoyancy field, it is highly accurate for the reference buoyancy field obtained by a three-dimensional sorting procedure. The second new technique builds on the local definition of E_{ap} in Holliday & McIntyre (1981). After using the improved sorting procedure to obtain a reference profile of buoyancy $b^*(z)$, this local definition is used to calculate the distributions of E_{ap} and its quadratic factor, the gravitational disturbance field $\mathscr{A}$. Evolution equations for E_{ap} and $\mathscr{A}$ are calculated with discrete consistency with the dynamical evolution of the buoyancy b in numerical simulations.

Local balances are mechanistically interpreted in terms of advective rearrangements of E_{ap} and $\mathscr{A}$, conversion with KE by vertical buoyancy flux wb and rearrangement and dissipation associated with buoyancy diffusion. Simple illustrations are presented for the non-rotating, viscous spin-down of an initially tilted buoyancy field to a state of rest with the reference profile $b^*(z)$ and for the effect of an overturning circulation on an initially unstable stratification.

The definition of $\mathscr{A}$ allows the calculation of the spectrum of E_{ap} and its dynamical balance equation, which in turn makes it possible to construct a complete picture of the fluctuation energy budget for both its kinetic and potential components. In an equilibrium Eady flow on scales smaller than the primary energy generation by baroclinic instability of the mean circulation, there is a buoyancy-flux conversion from E_{ap} to E_k associated with frontogenesis down to a scale set by frontal instability and frontogenetic arrest. On even finer cascades there are coupled inertial-cascade ranges with forward fluxes of both E_{ap} and E_k down to their dissipation at small scales, with spectrum exponents close to $-5/3$, nearly constant spectral fluxes and a negative conversion from E_k to E_{ap}. The characteristics of this rotating inertial range coincide with those previously shown for non-rotating, strongly stratified turbulence (Lindborg 2006; Lindborg & Brethouwer 2007), indicating the possibility of a continuous route to dissipation for APE in the general circulations of the atmosphere and ocean.

The new techniques make possible the study of energy balances and cross-scale transfers in both E_k and E_{ap} in computational simulations for all flows with buoyancy effects.

We appreciate discussion with Erik Linborg and Greet Brethouwer about their simulations of stratified turbulence. We thank a reviewer for advocating the desirability of the Appendix. This research was supported by the National Science Foundation through grants OCE 02-21177, OCE 03-36755 and OCE-0550227.

Appendix. Local energy balance

Consider the non-hydrostatic, incompressible Boussinesq equations with viscosity ν and buoyancy diffusivity μ and a reference profile $b^*(z, t)$ obtained from $b(x, y, z, t)$

by instantaneous adiatatic rearrangement. The substantial derivative of E_{ap} in (3.2) is

$$\begin{aligned}\frac{\mathrm{D}E_{ap}}{\mathrm{D}t} &= (\mathscr{Z}[b]-\mathscr{Z}[b^*])\,\frac{\mathrm{D}b}{\mathrm{D}t} - \left(\mathscr{Z}[b^*]-\mathscr{Z}[b^*]\right)\,\frac{\mathrm{D}b^*}{\mathrm{D}t} - \int_{b^*}^{b}\frac{\mathrm{d}\mathscr{Z}}{\mathrm{d}b}[b^*]\,\frac{\mathrm{D}b^*}{\mathrm{D}t}\,\mathrm{d}\tilde{b}\\ &= \mu(\mathscr{Z}[b]-\mathscr{Z}[b^*])\nabla^2 b - (b-b^*)\,\frac{\mathrm{d}\mathscr{Z}}{\mathrm{d}b}[b^*]\,\left(\frac{\partial b^*}{\partial t} - w\frac{\partial b^*}{\partial z}\right)\\ &= -w(b-b^*) - (b-b^*)\,\frac{\mathrm{d}\mathscr{Z}}{\mathrm{d}b}[b^*]\,\frac{\partial b^*}{\partial t}\\ &\quad + \mu\left(\nabla\cdot((\mathscr{Z}[b]-\mathscr{Z}[b^*])\nabla b) - \frac{\mathrm{d}\mathscr{Z}}{\mathrm{d}b}[b]\,(\nabla b)^2 + \frac{\partial b}{\partial z}\right). \end{aligned} \tag{A 1}$$

The middle right-hand-side term on the first line evidently vanishes, and we have made use of (3.1) and the identity

$$\frac{\mathrm{d}\mathscr{Z}}{\mathrm{d}b}[b^*]\frac{\partial b^*}{\partial z} = 1. \tag{A 2}$$

The right-hand side terms are the buoyancy-flux conversion to KE, an exchange because of the evolution of the reference state $b^*(z,t)$ and a diffusion effect that is partly sign definite and dissipative since $\mathrm{d}\mathscr{Z}/\mathrm{d}b \geqslant 0$. In the simple case of (3.1) the evolution of b^* is only due to diffusion. Thus, we identify the $-\boldsymbol{u}\cdot E_{ap}$ transferred from the left-hand side of (A 1) and the buoyancy-flux conversion as the advective influences $Adv\,[E_{ap}]$ and the second and third right-hand-side terms as the diffusive influences $Dif\,[E_{ap}]$ in the local APE balance.

The companion local KE balance equation is derived in a familiar way by taking the product of $\boldsymbol{u}$ with the momentum equation:

$$\frac{\mathrm{D}E_k}{\mathrm{D}t} = w(b-b^*) - \nabla\cdot((p-p^*)\boldsymbol{u}) + \nu(\nabla\cdot(\boldsymbol{u}\cdot\nabla\boldsymbol{u}) - (\nabla\boldsymbol{u})^2). \tag{A 3}$$

The first right-hand-side term is buoyancy flux conversion with the opposite sign as in (A 1); the second term is pressure flux divergence ($p-p^*$ is the excess pressure in the terminology of Holliday & McIntyre 1981, where $p^*(z,t)$ is in hydrostatic balance with b^*); and the third term is a viscosity effect that is partly sign definite and dissipative.

For $\mu=\nu=0$ and an invariant reference profile $b^*(z)$, the local energy balance simplifies to

$$\frac{\mathrm{D}}{\mathrm{D}t}(E_k + E_{ap}) = -\nabla\cdot((p-p^*)\boldsymbol{u}),$$

which is equivalent to (2.11) in Holliday & McIntyre (1981).

REFERENCES

Andrews, D. 1981 A note on potential energy density in a stratified compressible fluid. *J. Fluid Mech.* **107**, 227–236.

Bray, N. & Fofonoff, N. 1981 Available potential energy for MODE eddies. *J. Phys. Oceanogr.* **11**, 30–47.

Capet, X., McWilliams, J., Molemaker, M. & Shepetkin, A. 2008*a* Mesoscale to submesoscale transition in the California Current System: flow structure and eddy flux. *J. Phys. Oceanogr.* **38**, 29–43.

Capet, X., McWilliams, M., Molemaker, M. & Shepetkin, A. 2008*b* Mesoscale to submesoscale transition in the California Current System: frontal processes. *J. Phys. Oceanogr.* **38**, 44–64.

Charney, J. 1971 Geostrophic turbulence. *J. Atmos. Sci.* **28**, 1087–1095.

Eady, E. 1949 Long waves and cyclone waves. *Tellus* **1**, 33–52.

Henyey, F. S. 1983 Hamiltonian description of stratified fluid dynamics. *Phys. Fluids* **26**, 40–47.

Holliday, D. & McIntyre, M. 1981 On potential energy density in an incompressible, stratified flow. *J. Fluid Mech.* **107**, 221–225.

Huang, R. 1998 On available potential energy in a Boussinesq ocean. *J. Phys. Oceanogr.* **28**, 669–678.

Kaneda, Y., Ishihara, I., Yokokawa, M., Itakura, K. & Uno, A. 2003 Energy dissipation rate and energy spectrum in high resolution direct numerical simulation of turbulence in a periodic box. *Phys. Fluids* **15**, L21–L24.

Lindborg, E. 2006 The energy cascade in a strongly stratified fluid. *J. Fluid Mech.* **550**, 207–242.

Lindborg, E. & Brethouwer, G. 2007 Stratified turbulence forced in rotational and divergent modes. *J. Fluid Mech.* **586**, 83–108.

Lorenz, E. 1955 Available energy and the maintenance of the general circulation. *Tellus* **7**, 157–167.

Lorenz, E. 1967 *The Nature and Theory of the General Circulation of the Atmosphere*. World Meteorological Organization.

McDougall, T. 1987 Neutral surfaces. *J. Phys. Oceanogr.* **17**, 1950–1964.

Molemaker, M., McWilliams, J. & Yavneh, I. 2005 Baroclinic instability and loss of balance. *J. Phys. Oceanogr.* **35**, 1505–1517.

Molemaker, M., McWilliams, J. & Capet, X. 2010 Balanced and unbalanced routes to dissipation in equilibrated Eady flow. *J. Fluid Mech.* (in press).

Muller, P., McWilliams, J. & Molemaker, M. 2005 Routes to dissipation in the ocean: the 2D/3D turbulence conundrum. In *Marine Turbulence: Theories, Observations and Models* (ed. H. Baumert, J. Simpson & J. Sundermann), pp. 397–405. Cambridge University Press.

Pedlosky, J. 1987 *Geophysical Fluid Dynamics*. Springer.

Reid, R., Elliot, B. & Olson, D. 1981 Available potential energy: a clarification. *J. Phys. Oceanogr.* **11**, 15–30.

Riley, J. & Lindborg, E. 2008 Stratified turbulence: a possible interpretation of some geophysical turbulence measurements. *J. Atmos. Sci.* **65**, 2416–2424.

Shepherd, T. 1993 A unified theory of available potential energy. *Atmos.-Ocean* **31**, 1–26.

Stone, P. 1966 On non-geostrophic baroclinic instability. *J. Atmos. Sci.* **23**, 390–400.

Toole, J. 1998 Turbulent mixing in the ocean. In *Oceanic Modelling and Parameterization* (ed. E. Chassignet & J. Verron), vol. C 516, pp. 171–189, NATO Science Series. Kluwer Academic.

Tseng, Y.-H. & Ferziger, J. 2001 Mixing and available potential energy in stratified flows. *Phys. Fluids* **13**, 1281–1293.

Winters, K., Lombard, P., Riley, J. & D'Asaro, E. 1995 Available potential energy and mixing in density-stratified fluids. *J. Fluid Mech.* **289**, 115–128.